Geophysical Research Letters

RESEARCH LETTER
10.1029/2019GL082175

The Impact of Oxygen on the Reconnection Rate

P. Tenfjord[1], M. Hesse[1,2], C. Norgren[1], S. F. Spinnangr[1], and H. Kolstø[1]

[1]Birkeland Centre For Space Science, University of Bergen, Bergen, Norway, [2]Southwest Research Institute, San Antonio, TX, USA

Key Points:
- The presence of O^+ (or other heavy ions) significantly decreases the reconnection rate
- Demagnetized O^+ (and the associated electrons) acts as energy sink on the finite energy reservoir at the expense of protons
- The reduction in the reconnection rate follows a simple scaling that depends on the ratio of oxygen to proton concentration

Correspondence to:
P. Tenfjord,
paul.tenfjord@ift.uib.no

Citation:
Tenfjord, P., Hesse, M., Norgren, C., Spinnangr, S. F., & Kolstø, H. (2019). The impact of oxygen on the reconnection rate. *Geophysical Research Letters*, *46*, 6195–6203. https://doi.org/10.1029/2019GL082175

Received 23 JAN 2019
Accepted 22 MAY 2019
Accepted article online 29 MAY 2019
Published online 20 JUN 2019

Abstract We investigate the role of a background oxygen population in magnetic reconnection, using particle-in-cell simulations. We run several simulations, with different initial oxygen temperatures and densities, to understand how the reconnection rate is influenced, as oxygen is captured by the reconnection process. The oxygen remains approximately demagnetized on the relevant time and spatial scales and therefore has little *direct* (i.e., immediate mass loading) effect on the reconnection process itself. The reconnection rate is independent of the initial oxygen temperature but clearly dependent on the density. The reduced reconnection rate is twice as fast as predicted by mass loading. We describe a mechanism where the oxygen population (and the associated electrons) acts as an energy sink on the system, altering the energy partitioning. Based on a scaling analysis, we derive an estimate of the reconnection electric field that scales as $(1 + n_o/n_p)^{-1}$, where n_o and n_p is the oxygen and proton densities, respectively.

1. Introduction

Magnetic reconnection is the physical mechanism that facilitates the release of stored magnetic energy into kinetic energy of charged particles. This process occurs on very small spatial scales and involves intricate interactions between charged particles and fields in a region termed the diffusion region. In addition to protons (H^+) and electrons, many plasma systems include heavier species such as oxygen (O^+). In the magnetotail, the source of heavy ions is usually attributed to ionospheric outflow, which fills the magnetotail lobes with cold heavy ions (Haaland et al., 2012). Varying conditions in the inflow regions, such as different plasma populations or plasma properties, can impact the reconnection process. On both the dayside and nightside, observations show the involvement of additional cold, dense plasma or plasma beams (André et al., 2016; Borovsky & Denton, 2006; Fuselier et al., 2016; Kistler & Mouikis, 2016; Toledo-Redondo et al., 2017) can alter the reconnection process and eventually slow down the reconnection rate. Heavy ions like O^+ have larger Larmor radii than H^+ ions at the same velocities. This leads to a different kinetic behavior and additional scale lengths in the system (Divin et al., 2016; Shay & Swisdak, 2004; Toledo-Redondo et al., 2015). The presence of heavy ions can, if magnetized, mass load the system, and the resulting reduction of the Alfven velocity is believed to be a mechanism which can slow down reconnection (Hesse & Birn, 2004; Shay & Swisdak, 2004). In addition to the mass-loading effect, other mechanisms such as the effect of heavy ions of the tearing growth rate (Karimabadi et al., 2011) and induced ambipolar (charge-separation) electric fields (Liang et al., 2016, 2017) have been suggested. In addition to the new spatial scale, a new temporal scale exists as a result of the mass dependency on the cyclotron frequency. O^+ has a 16 times lower cyclotron frequency, which strongly influences the coupling to the magnetic field. Both the spatial and temporal scales must be considered to determine whether O^+ is magnetized. If the evolutionary time scale of the reconnection process is small compared to the oxygen cyclotron frequency, then the O^+ remains are effectively demagnetized and are therefore unable to mass load the system since it does not provide inertia to the inflow or outflow flux tubes. For a very large system, where the evolution can last longer, O^+ will likely become magnetized, and we expect the reconnection rate to scale as the inflow Alfven velocity (Shay & Swisdak, 2004). For shorter times scales, the kevolution is not clear.

In this manuscript we use 2.5-D particle-in-cell simulations to study the effect on the reconnection rate when a separate oxygen population is included in the inflow region. We ran a series of simulations designed to mimic an active magnetotail where ionospheric outflow has filled the lobes with O^+. Using different temperatures and number densities, we show how the reconnection rate is influenced. We show that the oxygen density has a significant effect on the reconnection rate, but it does not scale as expected from mass loading. Instead, the demagnetized O^+ behaves as an energy sink on the system, extracting energy that otherwise

would have been converted into mechanical energy of the protons. As a result, the reconnection rate is reduced, and the reduction depends on the oxygen density. Based on a scaling analysis of how the different species are energized, we arrive at a simple scaling that is in excellent agreement with the simulation results. Our results and predictions can prove valuable for understanding the dynamics of multispecies plasma near reconnection and for analyzing observations from, for example, NASA's Magnetospheric Multiscale Mission mission.

2. Simulation Setup

Our simulations are designed to mimic the magnetotail conditions during enhanced geomagnetic activity. During such conditions, ionospheric outflow from high latitudes enriches the magnetospheric lobes with cold oxygen. Spacecraft observation shows that the density of oxygen in the plasma sheet can be the dominating ion species during storm-time conditions (André & Cully, 2012; Kistler & Mouikis, 2016; Kistler et al., 2005, 2006; Mouikis et al., 2010). Ions originating from the ionosphere are expected to be cold, where observed temperatures range from 100 eV (Wygant et al., 2005) up to 260 eV (Seki et al., 1998). In comparison, plasma sheet protons typically have temperatures of several kiloelectron volts.

We employ a 2.5-D (two spatial components and three fields and velocity coordinates) particle-in-cell simulation, which has previously been applied to a variety of reconnection problems (e.g., Hesse et al., 2001; Tenfjord et al., 2018). The initial magnetic field configuration is a two-dimensional generalized Harris-type equilibrium (see Hesse & Birn, 2004, for details) with zero guide field. The initial magnetic field, defined as $B_x = B_0 \tanh(z/\lambda)$, where $\lambda = 2d_p$ is the half-width of the layer. All calculations use a proton/electron mass ratio of $m_\mathrm{p}/m_\mathrm{e} = 25$ and oxygen/ion mass ratio of $m_\mathrm{o}/m_\mathrm{p} = 16$. A total of $\sim 5 \cdot 10^9$ macroparticles is employed, divided equally between the species. Boundary conditions are periodic at $x = 0$ and $x = x_\mathrm{max}$. At the upper and lower boundaries, we employ specular reflection for particles, and the out-of-plane electric field is set to zero, implying flux conservation in the simulation domain.

Lengths are normalized to the proton inertial length: $d_p = c/\Omega_\mathrm{pi} \quad (= c\sqrt{\frac{m_\mathrm{p}}{4\pi n_\mathrm{p} e^2}} \quad)$. Time is normalized to the inverse of the proton cyclotron frequency: $\Omega_\mathrm{p}^{-1} \quad (= \frac{cm_\mathrm{p}}{eB})$. Our simulation domain size is $200 \times 50d_p$, divided into a grid of $3,200 \times 1,600$ cells. A time step of $\Omega_e \delta t = 1$ is employed. The density is normalized to the foreground current sheet density n_0. The velocity is normalized to the proton Alfven speed, based on n_0. The foreground temperatures fulfill $T_\mathrm{p} + T_\mathrm{e} = 0.5$ and proton/electron temperature $T_\mathrm{p}/T_\mathrm{e} = 5$. The ratio between the electron plasma frequency and gyro frequency is $\Omega_\mathrm{pe}/\Omega_\mathrm{ce} = 2$.

A uniformly distributed proton (H^+) background with $n_\mathrm{p} = 0.2$ is added to the Harris-sheet density distribution, which leads to a peak density of $n = 1.2$. In addition to the uniform H^+ population, oxygen populations with number densities ranging from $n_\mathrm{o} = 0$ to 0.4 are added to the inflow regions ("lobes"). The oxygen is inserted outside the current sheet at $|z| > 2.5d_p$, henceforth referred to as the initial oxygen boundary.

We use a total of six simulations, three of which have already been used to describe acceleration of oxygen and the formation of density striations (Tenfjord et al., 2018). These runs all had oxygen density $n_\mathrm{o} = 0.1$ and background proton density $n_\mathrm{p} = 0.2$, referred to as "$n_\mathrm{o} = 0.1$ run" with different temperatures. When a oxygen population with a finite temperature is added to the simulation, this additional pressure must be balanced by a reduction of the foreground temperature. For the "$n_\mathrm{o} = 0.1$ run ($T_\mathrm{o} = 200$ eV)," the foreground proton temperature has been reduced from $T_\mathrm{p} \approx 0.42 \quad [m \cdot V_A^2]$ ($T_\mathrm{e} = 0.08$) to $T_\mathrm{p} \approx 0.41$ ($T_\mathrm{e} = 0.05$) in simulation normalized units and the difference added to the oxygen (and associated electron) temperature. For the "$n_\mathrm{o} = 0.1$ run ($T_\mathrm{o} = 1$ keV)," the new foreground temperatures are $T_\mathrm{p} \approx 0.375 \quad [m \cdot V_A^2]$ ($T_\mathrm{e} = 0.05$). The three additional runs also have a uniform background proton population with density $n_\mathrm{p} = 0.2$ but with different oxygen densities. The "$n_o = 0.2$" and "$n_o = 0.4$" runs have oxygen densities of $n_\mathrm{o} = 0.2$ and $n_\mathrm{o} = 0.4$, respectively, and zero oxygen temperature. The "H^+ run" has no oxygen population but is otherwise equal to the runs that include oxygen. A detailed description of the simulation setup is found in Tenfjord et al. (2018).

3. Reconnection Rate

Based on a Sweet-Parker analysis, the reconnection rate scales with the Alfven velocity based on the total mass density in the system. From $V_\mathrm{in} \sim (\delta/L)V_A$, where V_in represents the inflow velocity, δ and L is the

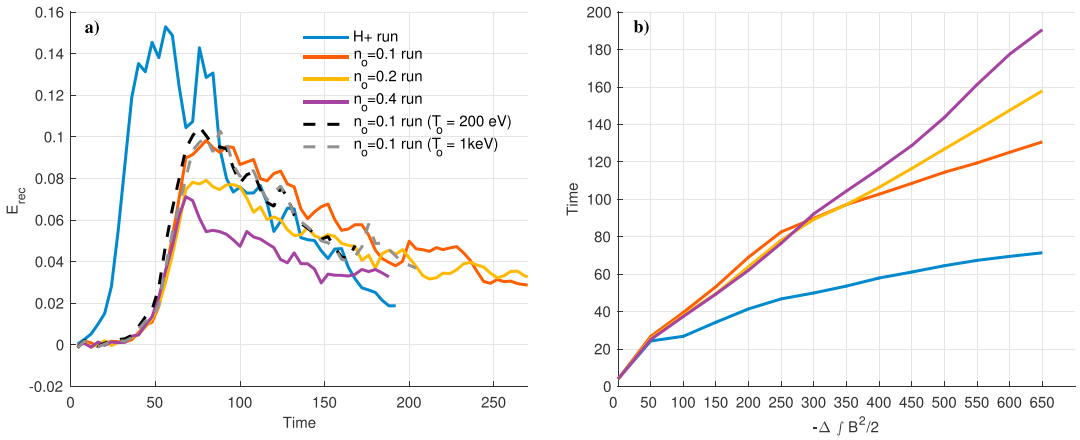

Figure 1. (a) Reconnection rate for the six simulations. (b) Overall magnetic energy in simulation domain as function of time. Magnetic energy defined as $\int B^2/2 \quad dxdz$. The initial magnetic energy is subtracted so that it represents the change in magnetic energy from the initial stage.

height and the width of the diffusion region, and the Alfven velocity ($V_A^2 = B^2/\rho\mu_0$) represents the outflow velocity. It follows that the reconnection rate is reduced as the mass increases (Alfven velocity decreases). This process is analogous to considering the flux tubes as more inert, so that more energy is spent on increasing the flux velocity when carried by a heavier mass. This requires that the plasma is magnetized.

Figure 1a shows the reconnection rate for our six simulations. Rate of reconnected flux is defined as $\frac{\mathrm{d}}{\mathrm{d}t}\Phi_{\mathrm{rec}} = \frac{\mathrm{d}}{\mathrm{d}t}\int \vec{B}\cdot\vec{n}da \left(=\int E_y \mathrm{d}y\right)$. The Alfven velocity used for normalization is based on the foreground proton number density in the current sheet at $t = 0$ and is thus equal for all runs. The run without oxygen (H^+ run) reaches a peak reconnection rate of nearly 0.15, while the runs including O^+ have a significantly lower rate, which is clearly dependent on the O^+ number density. Since the oxygen is inserted $2.5d_p$ above and below the current sheet at the start of the simulations, a transition period exists where reconnection proceeds with only H^+, before eventually the O^+ population is captured. The O^+ gets involved approximately at $t = 80$. This is particularly evident for the $n_o = 0.4$ run which has a peak rate of about 0.07 at $t = 70$, before reducing to ~0.055 at $t = 80$. The dashed lines show two simulations with the same number density $n_o = 0.1$ and temperatures of $T_o = 200\,\mathrm{eV}$ and $T_o = 1\mathrm{keV}$. The reconnection rate for these two runs that include temperature and the $n_o = 0.1$ run is close to identical, showing that the temperature does not have a significant effect on the reconnection rate. The values for the reconnection rates are summarized in Table 1 . Figure 1b shows time as a function of the decrease in integrated magnetic energy $\Delta U_B = 0.5\int (B^2(t=0) - B^2(t)) \quad dxdz$. The remaining figures are presented as a function of the total magnetic energy in the simulation domain. This allows us to compare the different runs at similar evolutionary stages, meaning each run has approximately reconnected the same amount of magnetic flux.

Based on the mass-loading effect, the reconnection rate should scale as the Alfven velocity of the total mass. Therefore, we expect the difference in the reconnection to scale like $\sqrt{(m_p n_p + m_o n_o)/(m_p n_p)}$. For the $n_o = 0.1$ run, which has a total mass density of $0.2m_p + 0.1m_o = 1.8m_p$, the expected reconnection rate would be ~0.05, while Figure 1a shows that it reconnects twice as fast (~0.1). The same is true for the other runs.

Table 1
For Each Simulation: Expected Reduction of Reconnection Based on Mass Loading, the Actual Reduction From Model, and E_y Scaling From Equation (14)

Runs	Expected reduction (rate)	Actual reduction (rate)	E_y scaling (equation (14))
H^+	1 (0.15)	1 (0.15)	1
$n_o = 0.1$	0.33 (0.05)	0.65(0.10)	0.66
$n_o = 0.2$	0.25 (0.037)	0.50 (0.078)	0.5
$n_o = 0.4$	0.18 (0.026)	0.35(0.055)	0.33

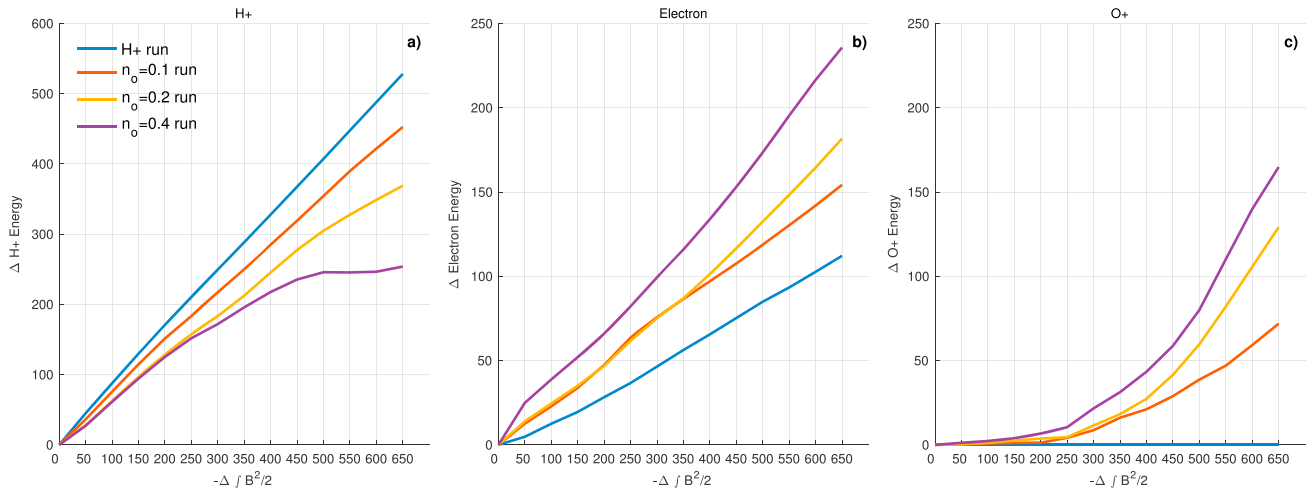

Figure 2. Energy distribution between the different populations. (a) Integrated mechanical (thermal and kinetic) energy of $H+$, (b) total electron energy, and (c) O^+ energy.

The inclusion of heavy ions introduce an additional time scale to the system due to the cyclotron frequency's mass dependence. Whether the oxygen is magnetized or not therefore depends on its temperature and the systems evolutionary time scale compared to the oxygen cyclotron frequency.

In our simulations, we find that the O^+ is dominated by electric forces and remains approximately demagnetized for all relevant timescales. Hence, if the evolutionary time scale of the reconnection process occurs on time scales much shorter than the O^+ cyclotron period, the reduction of the reconnection rate scales not as simple mass loading but through some different mechanism. Tenfjord et al. (2018) found that O^+ was ballistically accelerated, primarily by the Hall electric field (E_z). The authors also found that the O^+ did not play a direct role in the reconnection process; instead, the O^+ behaved approximately like "test-particles"—affected mainly by the present electric fields. Even though the O^+ population and associated electrons do not directly influence the reconnection process, they do extract energy from the fields that would otherwise be available for accelerating protons and electrons. In order to understand how the presence of the unmagnetized O^+ alters the energy partitioning, we proceed with an energy analysis in the simulation domain.

In Figure 2, we show the mechanical energy distribution between the different species as a function of $-\Delta \int B^2 \quad dxdz$. The mechanical energy represents the integrated kinetic and thermal energy over the entire domain, plotted as a function of magnetic energy. In Figure 2a, the blue line shows the amount of kinetic energy converted from magnetic energy for the run without O^+. Without any additional species, the acceleration and heating of the H^+ is the primary energy sink of the system. The sum of the H^+ and electron energy adds up to the magnetic energy spent. In Figure 2c, we see the energization of the O^+ population. The O^+, which is initially at rest, is captured by the reconnection process after about $-\Delta \int B^2/2 \quad dxdz = 250 (t \approx 80)$ and starts to significantly alter the energy partitioning. Since $n_e = n_o + n_p$, the additional electron concentration also becomes a significant energy sink (Figure 2b).

This demonstrates that even though the oxygen remains approximately demagnetized, both O^+ and the associated electron density still get energized and alter the energy partitioning of the system. This means that the O^+, along with the additional electron density, acts as an energy sink on the system. Since the electric fields must be self-consistently supported by any of the particle species, a reduction of the mechanical energy of the protons should be associated with a smaller reconnection electric field. In the next section, we test this hypothesis and investigate how the energization of the O^+ alters the reconnection rate.

4. How the Reconnection Rate Scales With Oxygen Density

In this section we present a physical scaling analysis, where the role of the energization of the different species are related to each other. Our analysis is based on the momentum equation of each species, and the final expressions are evaluated within the proton diffusion region, as a simple pressure balance argument. Since the electric fields need to be self-consistently supported by any of the particle species, the scaling

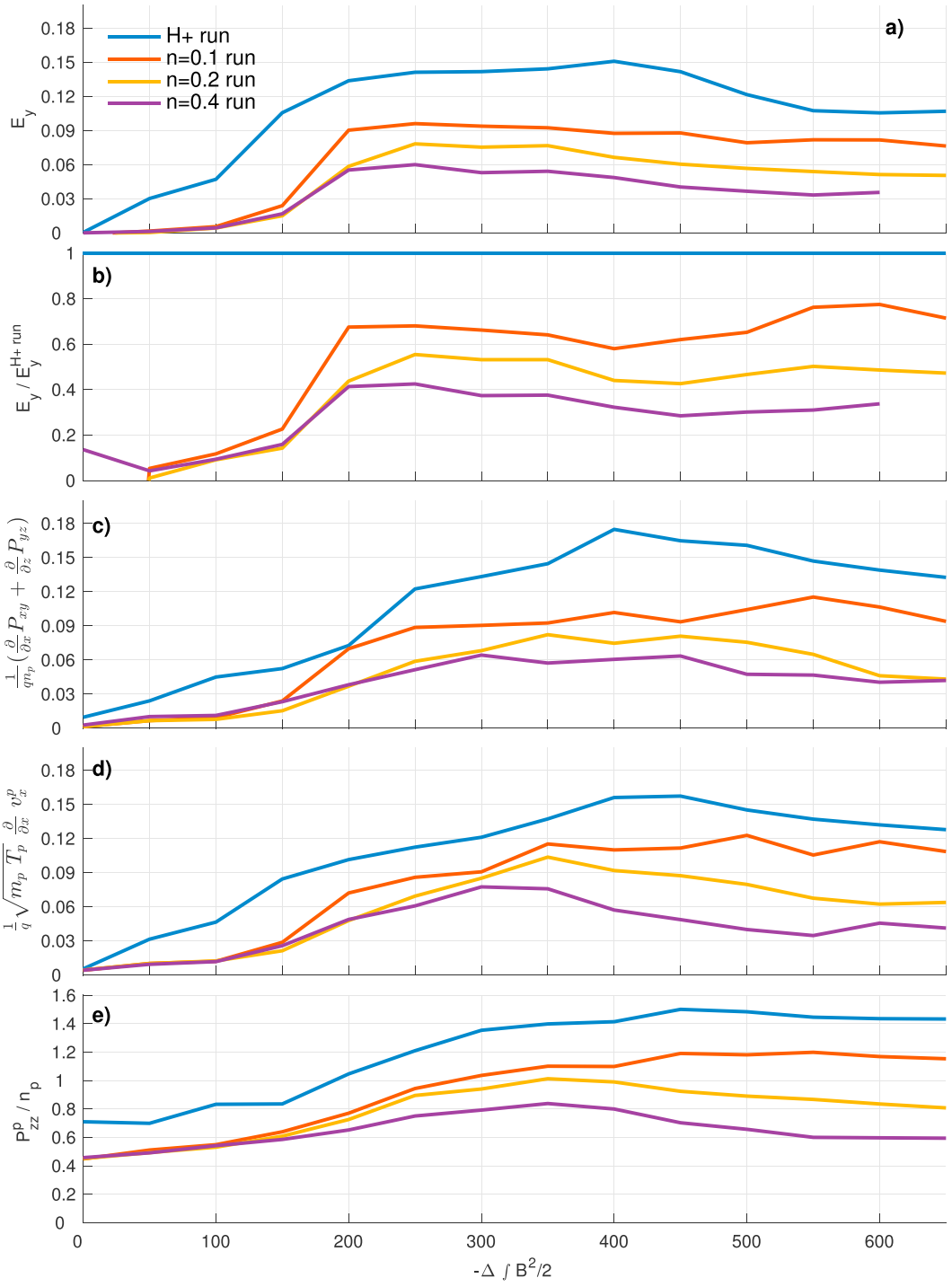

Figure 3. (a) Reconnection rate as shown in Figure 1 as a function of the change in magnetic energy. (b) Ratio between the four E_{rec} and $E_y^{H+\mathrm{run}}$ (reconnection rate for the H^+ run). (c) Reconnection rate estimated from the gradient of nongyrotropic pressure components in the proton diffusion region. (d) Reconnection rate estimated from equation (14) in (Hesse et al., 1999). (e) Reconnection rate estimated by P_{zz}.

analysis describes the effect on the reconnection electric field as an unmagnetized species extracts energy from the system. As expected, the scaling depends on the O^+ density, signifying that a higher concentration acts as a larger energy sink on the system, which results in a smaller reconnection electric field. Figure 3 shows several estimates for the reconnection rate E_y based on the proton species, all as a function of magnetic energy. Figure 3a is the reconnection rate as shown in Figure 1, while Figure 3b shows the ratio between each run and the baseline run. Figures 3c–Figure 3e (which will be discussed in the proceeding discussion) are calculated using the maximum value from a cut in the z direction through the reconnection site.

In order to develop a scaling relation for the reconnection rate, we begin by analyzing the proton momentum equation. In the proton diffusion region, the z component of the proton momentum equation is approximately:

$$E_z \sim \frac{1}{qn_\mathrm{p}} \frac{\partial}{\partial z} P^\mathrm{p}_{zz}, \tag{1}$$

where the terms have their usual meaning and the superscript specifies the species. The change in pressure from approximately zero to P^p_{zz} occurs over the scale of the Hall region, L_Hall, and is thus proportional to E_Z:

$$P^\mathrm{p}_{zz} \sim qn_\mathrm{p} L_\mathrm{Hall} E_Z. \tag{2}$$

The primary mechanism controlling the dissipation in the vicinity of the reconnection site is associated with nongyrotropic pressure effects with spatial scales comparable to the species Larmor radius (Hesse et al., 1999). While usually written for the electron species, the same must apply for the protons Kuznetsova et al. (2007). Thus, we express the reconnection electric field as a function of the nongyrotropic pressure component of the protons. In Figure 3c, the reconnection rate is estimated as the spatial derivatives of the nongyrotropic proton pressure (Hesse et al., 1999).

$$E_y \sim \frac{1}{qn_p} \left(\frac{\partial}{\partial x} P^\mathrm{p}_{xy} + \frac{\partial}{\partial z} P^\mathrm{p}_{zy} \right). \tag{3}$$

It is reasonable to assume that the nongyrotropic pressure tensor components depend linearly on the average kinetic energy, that is, on the trace of the tensor. If we further assume that the derivatives in equation (3) are of approximately the same magnitude and neglect the difference between P_{zz} and P_{xx}, we can write the reconnection electric field as

$$E_y \sim \frac{1}{qn_\mathrm{p}} \left(\beta \frac{P^\mathrm{p}_{zz}}{L_\mathrm{Hall}} \right) \tag{4}$$

where β is a proportionality constant relating the off-diagonal to the diagonal pressure term and L_Hall represents the scale length. Figure 3d shows the reconnection rate estimated from Hesse et al. (1998) and Kuznetsova et al. (1998), where the authors assumed a linear relationship between the nongyrotropic pressure tensor components and the trace of the tensor. Figure 3e shows the diagonal proton pressure divided by the proton density, and although the scales are different, the correlation to the actual rate is in good agreement.

We now arrive at an expression relating P^p_{zz} to the reconnection electric field:

$$P^\mathrm{p}_{zz} \sim qn_\mathrm{p} L_\mathrm{Hall} \frac{E_y}{\beta}. \tag{5}$$

By the same arguments as above, we can relate P^e_{zz} of the electrons to E_Y:

$$P^\mathrm{e}_{zz} \sim qn_\mathrm{e} L_\mathrm{EDR} \frac{E_y}{\alpha}. \tag{6}$$

The proportionality constant α relates the nongyrotropic and gyrotropic electron pressure, and the spatial derivative is estimated as the electron diffusion region (EDR) scale length, L_EDR. The kinetic energy gained by the oxygen particles is proportional to E_z. We make the simplifying assumption that, in the proton diffusion

region, this energization expresses itself primarily as thermal energy. We can then relate the energization of the oxygen to the Hall electric field, such that

$$P_{zz}^{\mathrm{O}} \sim q n_{\mathrm{o}} L_{\mathrm{Hall}} E_z, \tag{7}$$

where we have assumed that the associated length scale is equal to Hall L_{Hall}, since O^+ primarily gets energized by Hall E_z (proton diffusion region scale). Using equations (2) and (5), we can relate E_y to E_z:

$$E_y \sim \beta E_z. \tag{8}$$

This allows us to express P_{zz}^{O} as a function of E_y:

$$P_{zz}^{\mathrm{O}} \sim q n_{\mathrm{o}} L_{\mathrm{Hall}} \frac{E_y}{\beta}. \tag{9}$$

Equations (5), (6), and (9) represent the gyrotropic pressure of the protons, electrons, and O^+ as a function of the reconnection electric field E_y.

The magnetic field represents a finite energy source, and we now quantify how much energy is converted into the different species within the proton diffusion region. In the proton diffusion region, proton bulk flows are small; hence, the combined pressures of the protons, oxygen, and electrons balances the external magnetic pressure:

$$\frac{B^2}{2\mu_0} + P_{zz}^{\mathrm{p}} + P_{zz}^{\mathrm{e}} + P_{zz}^{\mathrm{O}} \sim const. \tag{10}$$

Substitute equations (5), (6), and (9) into equation (10),

$$\frac{B^2}{2\mu_0} + q n_{\mathrm{p}} L_{\mathrm{Hall}} \frac{E_y}{\beta} + q n_{\mathrm{e}} L_{\mathrm{EDR}} \frac{E_y}{\alpha} + q n_{\mathrm{o}} L_{\mathrm{Hall}} \frac{E_y}{\beta} \sim const. \tag{11}$$

Define $A_{\mathrm{e}} = q L_{\mathrm{EDR}}$ and $A_{\mathrm{p}} = q L_{\mathrm{Hall}}$, substitute $n_{\mathrm{e}} = n_{\mathrm{o}} + n_{\mathrm{p}}$, and simplify

$$\frac{B^2}{2\mu_0} + E_y \left(A_{\mathrm{p}} \beta^{-1} (n_{\mathrm{o}} + n_{\mathrm{p}}) + A_{\mathrm{e}} \alpha^{-1} (n_{\mathrm{o}} + n_{\mathrm{p}}) \right) \sim const. \tag{12}$$

If we define $A' = A_{\mathrm{p}} \beta^{-1} + A_{\mathrm{e}} \alpha^{-1}$ or $A' = q L_{\mathrm{Hall}} \beta^{-1} + q L_{\mathrm{EDR}} \alpha^{-1}$, this becomes

$$const - \frac{B^2}{2\mu_0} \sim A' E_y \left(n_{\mathrm{o}} + n_{\mathrm{p}} \right). \tag{13}$$

Note that the left-hand side and the constant A' do not depend on the oxygen concentration. Hence, we conclude that the reconnection electric field should scale like

$$E_y \sim \frac{1}{1 + \frac{n_{\mathrm{o}}}{n_{\mathrm{p}}}}. \tag{14}$$

In the first column of Table 1, we list the expected reduction of the reconnection rate (mass-loading effect: Alfven velocity of total mass) relative to the H^+ run and the expected reconnection rate in parentheses. The second column lists the actual reconnection rate reduction and rates, while the third column uses equation (14) to scale the rate. The actual and estimated reconnection rates are in excellent agreement.

In the above derivation, we assume that the O^+ population remains unmagnetized throughout the reconnection event. While this condition prevails throughout our entire simulation run, it seems clear that a longer-lasting reconnection process will eventually magnetize oxygen as well. In such a situation, the reduction should scale as the Alfven velocity of the total mass as the flux tubes becomes more inert. Therefore, the present energetically coupled situation constitutes a, perhaps, surprisingly long transitional phase.

5. Discussion and Summary

As we noted above, our scaling only applies for an unmagnetized species. In Earth's geospace, O^+ is the most likely candidate. In other planetary systems, the scaling should apply for other heavy unmagnetized species, such as SO_2 (Bodisch et al., 2017). Another interesting property of the scaling is its lack of mass dependency. This is a result of the lack of magnetization and simply means that a species with higher mass will be accelerated to a lower velocity—maintaining the same kinetic energy.

We have shown that when the plasma includes a heavy unmagnetized species, such as O^+, the reconnection rate is significantly reduced. If the heavier species are unmagnetized, the decrease in reconnection rate does not scale in the same way as simple mass loading. Specifically, the O^+ population remains demagnetized on time and spatial scales much larger then the evolutionary time scale of the reconnection process. Instead, the dynamics of O^+ is dominated by electric forces and acts as an energy sink on the total energy reservoir. Since the O^+ does not directly participate in the reconnection process, its role (along with the additional electrons) instead becomes to extract energy that would otherwise be available for the protons. If the reconnection process continues for an extended period of time, it is likely that the oxygen population will eventually become magnetized and mass load the system. Figure 1 shows the reconnection rate of the baseline run temporarily decreases between $t = 60$ and 75 (energy level 450–700), one may speculate whether the actual reconnection rate stays at 0.15, and in that case, the scaling at this time moves into direction of mass-loading scaling. An alternative interpretation could be that the second peak $t = 70$–90 represents the destruction of one or multiple islands which leads to a temporary increase in the reconnection rate. From this perspective, the reconnection rate scales more like our E_y-scaling (equation (14)), signifying that the oxygen is still demagnetized. The mechanism described in this manuscript differs from the mechanism proposed by Liang et al. (2016). The authors ran two simulations, one with equal number density of O^+ and H^+ and one simulation with H^+ only. The authors found that the reconnection rate is more than doubled for the simulation with H^+ only, compared to the simulation that included O^+. They propose that the reduced reconnection is a result of the oxygen inertia which encumbers the outflow and that ambipolar electric fields are set up to accelerate the O^+. Based on equation (14), our scaling predicts that the reconnection should reduce by 50%, which is close to their ∼43% reduction—a result indicating that the oxygen energy sink may play a role in their model as well. Other studies investigating the role of O^+ on the reconnection rate commonly employ equal mass density setups such that the Alfven velocity is unchanged, and other effects of O^+ may be studied (e.g., Hesse et al., 2001; Markidis et al., 2011). For equal mass density on our scaling, equation (14) predicts that the reconnection rate is reduced by only 5%, meaning that the O^+ did not become a significant energy sink in the system and is thereby unable to significantly affect the reconnection rate. Whether O^+ is magnetized should be determined by standard criteria, for example, ratio gradient scale length compared to larmor radius, or in our case, an additional criterion is related to a comparison of the evolution time scale to the larmor cyclotron time for the oxygen, whenever feasible. In light of these results, it may be necessary to consider the oxygen population as demagnetized and not being able to mass load the reconnection process. This depends on the evolutionary stage the reconnection process currently is at; if early in the evolution or if the reconnection event is bursty, it is reasonable to believe that the reconnection will scale as dictated by equation (14).

Our findings are summarized as follows.

1. The presence of O^+ (or other heavy ions) significantly decreases the reconnection rate.
2. The O^+ temperature has no significant effect.
3. Additional plasma species (and the associated electrons) alters the energy deposition between the species and depending on the concentration becomes a major energy sink.
4. Based on a scaling analysis we found, in agreement with the simulations, that the reduction of the reconnection rate scales like $\frac{1}{(1+n_o/n_p)}$.

Our results predict the impact of a cold oxygen population of reconnection in the magnetotail and other environments. We hope that they will stimulate research based on space mission data, in particular the Magnetospheric Multiscale mission.

Acknowledgments
This study was supported by the Research Council of Norway/CoE under contract 223252/F50, by NOTUR/NORSTOR under project NN9496K, and by NASA's MMS mission.

References

André, M., & Cully, C. M. (2012). Low-energy ions: A previously hidden solar system particle population. *Geophysical Research Letters*, *39*, L03101. https://doi.org/10.1029/2011GL050242

André, M., Li, W., Toledo-Redondo, S., Khotyaintsev, Y. V., Vaivads, A., Graham, D. B., et al. (2016). Magnetic reconnection and modification of the Hall physics due to cold ions at the magnetopause. *Geophysical Research Letters*, *43*, 6705–6712. https://doi.org/10.1002/2016GL069665

Bodisch, K. M., Dougherty, L. P., & Bagenal, F. (2017). Survey of Voyager plasma science ions at Jupiter: 3. Protons and minor ions. *Journal of Geophysical Research: Space Physics*, *122*, 8277–8294. https://doi.org/10.1002/2017JA024148

Borovsky, J. E., & Denton, M. H. (2006). Effect of plasmaspheric drainage plumes on solar-wind/magnetosphere coupling. *Geophysical Research Letters*, *33*, L20101. https://doi.org/10.1029/2006GL026519

Divin, A., Khotyaintsev, Y. V., Vaivads, A., André, M., Toledo-Redondo, S., Markidis, S., & Lapenta, G. (2016). Three-scale structure of diffusion region in the presence of cold ions. *Journal of Geophysical Research: Space Physics*, *121*, 12,001–12,013. https://doi.org/10.1002/2016JA023606

Fuselier, S. A., Burch, J. L., Cassak, P. A., Goldstein, J., Gomez, R. G., Goodrich, K., et al. (2016). Magnetospheric ion influence on magnetic reconnection at the duskside magnetopause. *Geophysical Research Letters*, *43*, 1435–1442. https://doi.org/10.1002/2015GL067358

Haaland, S., Li, K., Eriksson, A., André, M., Engwall, E., Förster, M., et al. (2012). Cold ion outflow as a source of plasma for the magnetosphere. *Geophysical Monograph Series*, *199*, 341–353. https://doi.org/10.1029/2012GM001317

Hesse, M., & Birn, J. (2004). On the cessation of magnetic reconnection. *Annales Geophysicae*, *22*, 603–612.

Hesse, M., Kuznetsova, M., & Birn, J. (2001). Particle-in-cell simulations of three-dimensional collisonless magnetic reconnecion. *Journal of Geophysical Research*, *106*(A12), 29831. https://doi.org/10.1029/2001JA000075

Hesse, M., Neukirch, T., Schindler, K., Kuznetsova, M., & Zenitani, S. (1999). The diffusion region in collisionless magnetic reconnection. *Physics of Plasmas*, *6*, 3–23. https://doi.org/10.1063/1.873436

Hesse, M., Winske, D., & Birn, J. (1998). On the ion-scale structure of thin current sheets in the magnetotail. *Physica Scripta*, *T74*, 63–66. https://doi.org/10.1088/0031-8949/1998/T74/012

Karimabadi, H., Roytershteyn, V., Mouikis, C. G., Kistler, L. M., & Daughton, W. (2011). Flushing effect in reconnection: Effects of minority species of oxygen ions. *Planetary and Space Science*, *59*(7), 526–536. https://doi.org/10.1016/j.pss.2010.07.014

Kistler, L. M., & Mouikis, C. G. (2016). The inner magnetosphere ion composition and local time distribution over a solar cycle. *Journal of Geophysical Research: Space Physics*, *121*, 2009–2032. https://doi.org/10.1002/2015JA021883

Kistler, L. M., Mouikis, C. G., Cao, X., Frey, H., Klecker, B., Dandouras, I., et al. (2006). Ion composition and pressure changes in storm time and nonstorm substorms in the vicinity of the near-Earth neutral line. *Journal of Geophysical Research*, *111*, 1–12. https://doi.org/10.1029/2006JA011939

Kistler, L. M., Mouikis, C., Möbius, E., Klecker, B., Sauvaud, J. A., Réme, H., et al. (2005). Contribution of nonadiabatic ions to the cross-tail current in an O^+ dominated thin current sheet. *Journal of Geophysical Research*, *110*, A06213. https://doi.org/10.1029/2004JA010653

Kuznetsova, M. M., Hesse, M., Rastätter, L., Taktakishvili, A., Toth, G., De Zeeuw, D. L., et al. (2007). Multiscale modeling of magnetospheric reconnection. *Journal of Geophysical Research*, *112*, 1–15. https://doi.org/10.1029/2007JA012316

Kuznetsova, M. M., Hesse, M., & Winske, D. (1998). Kinetic quasi-viscous and bulk flow inertia effects in collisionless magnetotail reconnection. *Journal of Geophysical Research*, *103*(A1), 199–213. https://doi.org/10.1029/97JA02699

Liang, H., Ashour-Abdalla, M., Lapenta, G., & Walker, R. J. (2016). Oxygen impacts on dipolarization fronts and reconnection rate. *Journal of Geophysical Research: Space Physics*, *121*, 1148–1166. https://doi.org/10.1002/2015JA021747

Liang, H., Lapenta, G., Walker, R. J., Schriver, D., El-Alaoui, M., & Berchem, J. (2017). Oxygen acceleration in magnetotail reconnection. *Journal of Geophysical Research: Space Physics*, *122*, 618–639. https://doi.org/10.1002/2016JA023060

Markidis, S., Lapenta, G., Bettarini, L., Goldman, M., Newman, D., & Andersson, L. (2011). Kinetic simulations of magnetic reconnection in presence of a background O^+ population. *Journal of Geophysical Research*, *116*, 1–13. https://doi.org/10.1029/2011JA016429

Mouikis, C. G., Kistler, L. M., Liu, Y. H., Klecker, B., Korth, A., & Dandouras, I. (2010). H^+ and O^+ content of the plasma sheet at 15–19 Re as a function of geomagnetic and solar activity. *Journal of Geophysical Research*, *115*, 1–12. https://doi.org/10.1029/2010JA015978

Seki, K., Terasawa, T., Hirahara, M., & Mukai, T. (1998). Quantification of tailward cold O^+ beams in the lobe/mantle regions with Geotail data: Constraints on polar O^+ outflows. *Journal of Geophysical Research*, *103*(A12), 29,371–29,381. https://doi.org/10.1029/98JA02463

Shay, M. A., & Swisdak, M. (2004). Three-species collisionless reconnection: Effect of O^+ on magnetotail reconnection. *Physical Review Letters*, *93*(17), 4–7. https://doi.org/10.1103/PhysRevLett.93.175001

Tenfjord, P., Hesse, M., & Norgren, C. (2018). The formation of an oxygen wave by magnetic reconnection. *Journal of Geophysical Research: Space Physics*, *123*, 9370–9380. https://doi.org/10.1029/2018JA026026

Toledo-Redondo, S., André, M., Khotyaintsev, Y. V., Lavraud, B., Vaivads, A., Graham, D. B., et al. (2017). Energy budget and mechanisms of cold ion heating in asymmetric magnetic reconnection. *Journal of Geophysical Research: Space Physics*, *122*, 9396–9413. https://doi.org/10.1002/2017JA024553

Toledo-Redondo, S., Vaivads, A., André, M., & Khotyaintsev, Y. V. (2015). Modification of the Hall physics in magnetic reconnection due to cold ions at the Earth's magnetopause. *Geophysical Research Letters*, *42*, 6146–6154. https://doi.org/10.1002/2015GL065129

Wygant, J. R., Cattell, C. A., Lysak, R., Song, Y., Dombeck, J., Mcfadden, J., et al. (2005). Cluster observations of an intense normal component of the electric field at a thin reconnecting current sheet in the tail and its role in the shock-like acceleration of the ion fluid into the separatrix region. *Journal of Geophysical Research*, *110*, 1–30. https://doi.org/10.1029/2004JA010708